MODELING AND FIELD ANALYSIS OF THE LEIR BENDING MAGNETS AND OPTICS INTEGRATION

H. Deveci, M. A. Jebramcik
1211 CERN, Geneva, Switzerland

Abstract

This contribution presents the modelling of the dipole magnets of the Low-Energy Ion Ring (LEIR) at CERN. The LEIR dipoles are iron-dominated C-type 90° sector magnets. Each LEIR dipole consists of six blocks of roughly 1 m-long laminated steel yoke with copper coils. The main challenges of the design stem from the axial air gaps and the varying angles between the blocks, which cause unwanted harmonics in the magnetic field. These aspects lead to mismatches between measured and predicted linear optics parameters in LEIR. Due to the unconventional magnet design, efforts are made to obtain three-dimensional field maps and multipole field components with high accuracy. The study began with 2D Finite Element Analysis (FEA) in different cross sections and continued with 3D FEA for the examination of the integrated field and the multipole components. The FEA is computed using different programs for cross-comparison and to increase the model accuracy by fine-tuning. Finally, the results have been integrated into optics codes, and the linear optics is compared with linear optics measurements.

INTRODUCTION

The Low Energy Ion Ring (LEIR) [1] is a key element of the heavy-ion injector chain at CERN. It receives long pulses of lead ions from Linear Accelerator 3 (Linac 3) and converts them into short, high-intensity bunches suitable for further acceleration toward the Large Hadron Collider (LHC). After the RF capture, the bunches are accelerated from an energy of 4.2 MeV per nucleon up to 72 MeV per nucleon over a cycle time of 3.6 s. At extraction, the beam energy is appropriate for transfer to the Proton Synchrotron (PS), where the ions are accumulated and further accelerated.

LEIR was proposed in 1993 as a conversion of the existing Low Energy Antiproton Ring (LEAR) [2]. Optics measurements have historically indicated a mismatch between assumed (model) beam optics and actual beam optics in LEIR [3]. It has been the subject of speculation whether the potential cause for the mismatch between the measured and model beam optics is caused by an incorrect modeling of the bending magnets within the used tracking codes. For these reasons, efforts are being made to obtain exact field maps of the bending magnets to enable a more accurate implementation into tracking codes. The geometry of the bending magnets is characterized by multiple air gaps between magnetic blocks, non-uniform edge orientations, and a gap width that varies along the magnet length. These features significantly increase the complexity of both field computation and accurate numerical modeling [3]. In the context of LEIR, there are additional challenges, such as limited availability of detailed documentation and validated legacy models that are needed for the modeling of magnets using state-of-the-art simulation software.

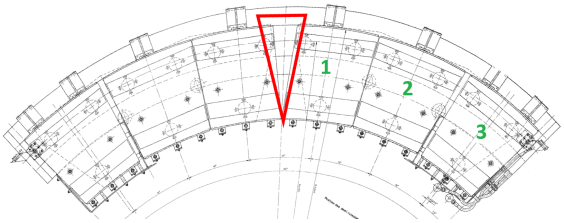

Figure 1: Top view of the LEIR dipole [4].

The LEIR dipole is an iron-dominated, water-cooled resistive magnet. Its mechanical structure is composed of six independent yoke blocks and a single curved bedstead coil extending over the full magnet length. In addition to the main coil, the two outermost blocks also include pole-face windings and back-leg windings. This configuration provides additional degrees of freedom for field shaping and correction, but further increases the complexity of the electromagnetic modeling. Figure 1 is an assembly drawing showing the top view of the magnet, including the yoke blocks, main winding, and the auxiliary equipment. The air gap in the middle is highlighted, as it is critically important for the harmonic content. The yoke blocks are numbered from the centre outward.

Another feature of the outermost yoke blocks is that they have a slightly larger aperture than the remaining yokes, resulting in a lower central magnetic field. Table 1 lists the main parameters of the LEIR dipoles.

Table 1: Parameters of the LEIR Dipole

Parameter	Units	Value
Current at injection / extraction	A	770 / 3290
Resistance at 20 °C	mΩ	6
Inductance	mH	25
Pole gap of central / lateral blocks	mm	80 / 88
Total length	mm	6378
Turns main / back-leg winding		12 / 10

MODELLING AND FEA

A comparative analysis has been performed using parametric models developed in Ansys Maxwell and OPERA. The modelling studies began with 2D and continued with 3D magnetostatic analyses. The pole-face windings and the back-leg windings have not been included in the initial sim-

ulations, as they are inactive in steady-state operation. The obtained results have been validated against B-train measurements within 1 % of margin, indicating that they are more precise than their predecessors.

2D Models

Figure 2 (left) shows the top half of the cross-section of the central blocks at high-field excitation, corresponding to the extraction energy (72 MeV/nucleon) and a 1.23 T central field. For the outermost block, the central field is 1.12 T due to the aforementioned increase in the aperture. Despite local saturation in the corners of the yoke, the general behaviour of the magnet indicates that it remains in the linear region of the B–H curve. This is an expected result, as the maximum current of this magnet was 5 kA historically, corresponding to a 1.6 T central field during LEAR operation. No noticeable difference is observed between the field density contour plots of the central and outermost yoke blocks, as the only distinction between these blocks is a 10 % difference in the aperture height.

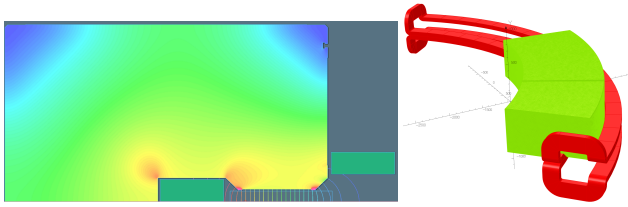

Figure 2: Left: Top half of the cross-section of the first two blocks of the LEIR dipole. Purple (blue) corresponds to 2 T (~0 T). Right: 3D OPERA model of one magnet sector.

The magnetic field density in the midplane at extraction energy shows excellent agreement with a 99.99 % accuracy between Ansys Maxwell and OPERA, with a central field of 1.232 T for the first two blocks and 1.122 T for the third block. A similar agreement has been obtained at injection energy, with a central field of 288 mT for the central block cross-section and 262 mT for the outermost block cross-section.

3D Models

Following the 2D simulations, an extensive 3D parametric model was created in OPERA. To simplify the model and reduce simulation time, a quarter of the magnet is included by exploiting symmetry, notably in the ZX and XY planes. The XY plane is the midplane cutting the top view, enabling the modelling of three blocks instead of six, as described in the previous section and visible in Fig. 1. The ZX plane bisects the magnet cross-section, as shown in Fig. 2 (left). An additional simplification that allows stable models to be obtained without compromising accuracy is to model the first two blocks as a single one. The axial air gap between the first two blocks (~ 1 mm) is negligible for a magnet of this length (stack length > 6 m). Figure 2 (right) shows the 3D model in OPERA. The coil is represented in full, as it is not modelled as a solid body.

Figure 3 shows the magnetic field density in the midplane at extraction energy, comparing the 3D and 2D analysis results. The mid-slices of each block in the 3D model correspond to angular positions of 7.5°, 22.5°, and 37.5° from the magnet centre, respectively, which can be compared directly with the 2D results for the central and outermost blocks. Since the fields in the midplane at 7.5° and 22.5° match almost exactly, only one is shown for clarity.

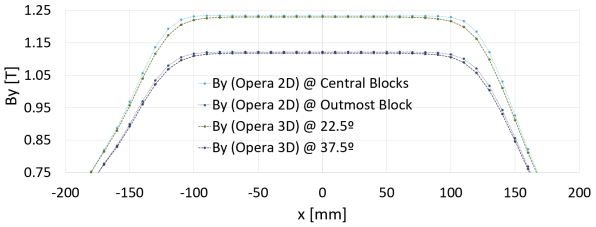

Figure 3: Magnetic field density in the midplane at extraction energy: comparison between 2D and 3D results.

Figure 4 shows the variation of the vertical magnetic field component, B_y, along the ideal trajectory through the yoke. Note that the yoke covers slightly more than 90°. The effect of the increased air gap in the outermost yoke blocks is clearly visible. In addition, the field decreases to approximately 30% of its peak value across the central air gap. The same characteristic is observed at the extraction energy.

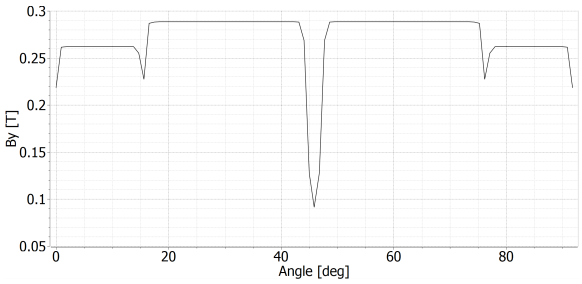

Figure 4: Variation of B_y along the magnetic centre of the magnet through the yoke at injection energy.

HARMONIC ANALYSIS

The multipole components have been calculated via Discrete Fourier Transformation (DFT) on a circle of 30 mm radius in the aperture, centred on the magnetic centre of the magnet [5]. For 2D analysis, one circle per cross-section is sufficient. This circle is sampled at 360 equally spaced points. For the 3D model, the same analysis has been performed repeatedly by discretising the magnet into thin slices longitudinally. The step size is set to 0.25° assuming a central radius of R = 4.17 m, corresponding to approximately 180 slices over the full 45° arc of the symmetry model. Note that the full 90° arc is used for the beam trajectory, as this represents the main beam path. The yoke extends slightly beyond 90° due to the wedge angles at the block ends.

At injection energy, the B_2 component amounts to approximately 0.8 units on the analysis radius, with significantly smaller higher-order components. At extraction energy, the B_2 component reaches approximately 1.8 units, again with small higher-order components. The change in cross-section

results in only minor variations, and the multipole spectra from the 2D and 3D analyses are in excellent agreement.

Figure 5 shows the harmonic spectrum from the 2D and 3D analyses at both injection and extraction energies. A similar agreement is observed for the outermost block cross-section and the corresponding 3D slice at 37.5°.

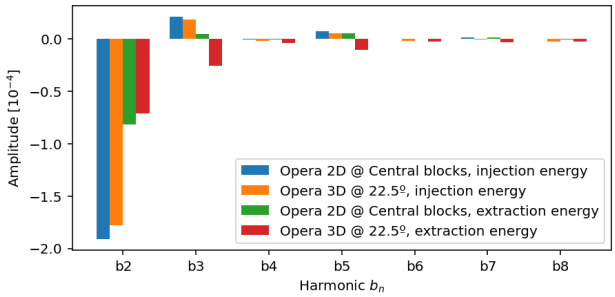

Figure 5: Harmonic components from 2D analysis of the central block cross-section and the corresponding 3D slice at 22.5°, at injection and extraction energies.

The harmonic analysis of the 3D results at the magnet extremities, and at the centre of the large axial air gap, reveals significantly enhanced harmonic components. For example, the b_2 component reaches −338 units in the air gap at 0°, and between 10 and 40 units at the end of the yoke at 45°, depending on the excitation current. The same harmonic analysis has also been carried out in the fringe-field region by extending the integration path beyond the end of the yoke. At $s = 430$ mm, the main dipole field has decayed to less than 2.5 % of its peak value. The fringe-field region is sampled with 92 equally spaced steps in the post-processing.

INTEGRATION INTO XSUITE

Before any field map information can be integrated into an Xsuite model, the correct beam path through the field map must be determined by integrating the Lorentz force. The analysis shows that the beam is displaced by approximately 4 cm with respect to a constant bending radius toward the inside of the magnet, since the magnetic field is initially weaker (block 3, with increased pole gap) and subsequently stronger (blocks 1 and 2). This behaviour was also seen in BDSIM with direct tracking through field maps. Aperture measurements have qualitatively confirmed reduced apertures toward the inside of the bending magnets.

The modelling of the bending magnets and the beam-path analysis has also revealed apparent inconsistencies in the current optics model. At injection energy, the following corrections to the model were identified: a) the entrance angle at block 3 is $e_1 = 15$ mrad instead of 12 mrad; b) the exit angle at block 1 is $e_2 = -131$ mrad instead of −96 mrad; c) the effective magnet length (beam path) is reduced by 3 cm, corresponding to a change in circumference of 12 cm; d) the FINT integrals [6], previously set to zero, contribute to the focusing of the beam and are found to sum to $\sum_i \mathrm{FINT}_i = 1.6$, accounting for contributions from the edges of blocks 1 and 3 with fringe-field-like field roll-offs; e) quadrupole and sextupole components have been attributed to the different parts of the magnets as shown in Fig. 6.

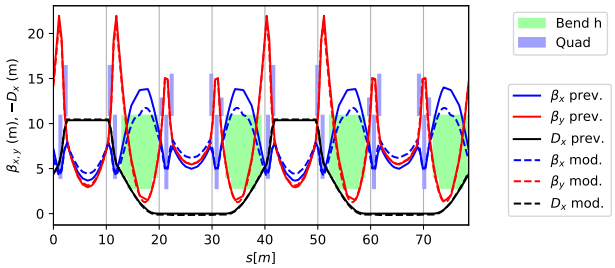

Figure 6: $K1$ and $K2$ components along the bending magnet. Components in fringes are nullified and are covered by FINT.

The analysis and the effects of these changes of the dipole model are still being investigated. The most prominent change is a reduction of β_x within the bending magnets by several metres at injection energy (see Fig.7). A first analysis appears to indicate smaller optics changes at extraction energy although optics measurements at top energy have yielded large deviations with respect to the optics model historically. Extracting the beam optics from the orbit-response matrix via COBEA [7, 8] was attempted in the 2025 Run for the first time. The optics changes appear to reduce the observed beta-beating during those measurements.

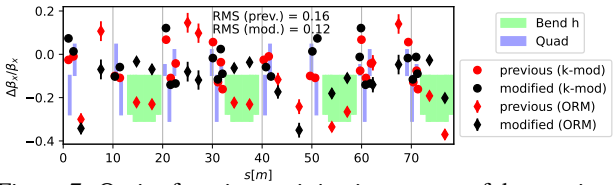

Figure 7: Optics functions at injection energy of the previous and modified models without the local e-cooler settings.

CONCLUSION & OUTLOOK

The modelling of the LEIR bending magnets has been highly successful: the simulated fields at injection and extraction energy are in good agreement with measurements (B-train) and prior simulations. Obtaining the field maps and studying the magnet geometry have already led to an optics model that is expected to lead to reduced beta-beating at injection energy. The optics analysis will be extended to extraction energy that was more critical in the past; however, the modification of the optics appears to be smaller there. The impact on the aperture model, transient electromagnetic analysis to see the effects of the eddy currents and hysteresis, and the change in circumference will be investigated further in 2026.

REFERENCES

[1] CERN, "Low-Energy Ion Ring (LEIR)," `https://home.cern/science/accelerators/low-energy-ion-ring` [Accessed: Apr. 2025].

[2] CERN, "Low-Energy Antiproton Ring (LEAR)," https://home.cern/science/accelerators/low-energy-antiproton-ring [Accessed: Apr. 2025].

[3] F. Carlier *et al.*, "Towards optics measurements with a new LEIR BPM system," in *Proc. 14th Int. Particle Accelerator Conf. (IPAC'23)*, Venice, Italy, May 2023, pp. 1644–1647. doi:10.18429/JACoW-IPAC2023-TUPA150

[4] CERN Engineering & Equipment Data Management Service (EDMS), "Drawings folder for PXMBHEGHWP, Assembly Drawing E10.1137.0," Document No. 1565229942, 1982. https://edms.cern.ch/ui/#!master/navigator/document?D:1565229942:1565229942:subDocs [Accessed: Apr. 2025].

[5] S. Russenschuck, *Field Computation for Accelerator Magnets: Analytical and Numerical Methods for Electromagnetic Design and Optimization*, 2nd ed. Weinheim, Germany: Wiley-VCH, 2010, ch. 6, pp. 237–268. doi:10.1002/9783527635467

[6] K. L. Brown, "A first- and second-order matrix theory for the design of beam transport systems and charged particle spectrometers," SLAC National Accelerator Laboratory, Menlo Park, CA, USA, Tech. Rep. SLAC-75, 1967.

[7] B. Riemann *et al.*, "Validating the COBEA algorithm at the DELTA storage ring," in *Proc. 9th Int. Particle Accelerator Conf. (IPAC'18)*, Vancouver, Canada, Apr.–May 2018, pp. 4611–4614. doi:10.18429/JACoW-IPAC2018-THPML084

[8] B. Riemann *et al.*, "COBEA - optical parameters from response matrices without knowledge of magnet strengths," in *Proc. 8th Int. Particle Accelerator Conf. (IPAC'17)*, Copenhagen, Denmark, May 2017, pp. 1069–1072. doi:10.18429/JACoW-IPAC2017-MOPIK066